Exploring dynamic dimers for singlet fission in thiophene-functionalized pentacene derivatives

PAPER • OPEN ACCESS

Exploring dynamic dimers for singlet fission in thiophene-functionalized pentacene derivatives

Journal of Physics: Materials

OPEN ACCESS

RECEIVED
31 January 2026

REVISED
11 June 2026

ACCEPTED FOR PUBLICATION
28 July 2026

PUBLISHED
18 August 2026

PAPER

Exploring dynamic dimers for singlet fission in thiophene-functionalized pentacene derivatives

Hanna Larsson[1,2], **Hassan Mourad**[1], **Maureen Gumbo**[1], **Andrew B Maurer**[1,3,4,*] and **Maria Abrahamsson**[1,2,*]

[1] Department of Chemistry and Chemical Engineering, Chalmers University of Technology, Gothenburg, Sweden
[2] Wallenberg Initiative Materials Science for Sustainability, Department Chemistry and Chemical Engineering, Chalmers University of Technology, Gothenburg, Sweden
[3] Department of Chemistry and Schiller Institute for Integrated Science and Society, Boston College, Chestnut Hill, MA 02467, United States of America
[4] Advanced Photon Source, Argonne National Laboratory, Lemont, IL 60439, United States of America
[*] Authors to whom any correspondence should be addressed.

E-mail: amaurer@anl.gov and abmaria@chalmers.se

Keywords: singlet fission, chromophore–chromophore interactions, pentacene derivatives, dynamic dimer, femtosecond transient absorption, photophysics

Supplementary material for this article is available online

Abstract

Singlet fission (SF) is a spin-allowed photophysical process of considerable interest for next-generation solar-energy conversion. Orientation, proximity and orbital overlap of the chromophores largely affect the success of SF, which can be overcome by forming covalent-linked dimers. However, triplet separation then becomes a key challenge for efficient SF. Therefore, we are introducing a dynamic, non-covalent dimer strategy, that enables effective SF without requiring covalent linkers or solid-state packing. The chromophores associate only through weak intermolecular interactions forming dynamic dimers, still able to undergo SF. Two TIPS-pentacene derivatives functionalized with a thiophene unit at the 2-position, bearing either an aldehyde (PTA) or a carboxylic acid (PTCA), were synthesized to promote π-stacking and hydrogen bonding. Comprehensive photophysical characterization shows that both compounds can undergo efficient SF even at micromolar concentrations, with initial rates of 1.3×10^{11} and 5.6×10^{10} s^{-1}, respectively. Furthermore, unlike covalent dimers or crystalline systems, our approach facilitates tunability of the excited-state dynamics by concentrations, pH, and the introduction of cations that form dynamic ion-bridges through weak coordination. These results demonstrate that dynamic, non-covalent assemblies offer a versatile platform for modulating SF in solution and opening new avenues for designing adaptive SF materials.

1. Introduction

The utilization of photovoltaics (PV) has increased rapidly over the past decade and is expected to be central to the transition toward greater reliance on renewable energy [1, 2]. This has spurred interest in developing more efficient solar cells and consequently, ways to overcome the thermodynamic limit, the so-called Shockley–Queisser limit, which is ca. 34% for single junction silicon solar cells [3]. One strategy to circumvent the efficiency limit is to increase the total energy extracted from high energy photons through the incorporation of singlet fission (SF) materials with PV devices [4–6].

SF is a spin-allowed process, that occurs when a singlet excited-state (S_1) chromophore interacts favorably with a ground-state chromophore to form a so-called correlated triplet–triplet pair, with overall singlet character, $^1(TT)$ [7]. If this correlated triplet pair is further transformed into two independent triplet states (T_1), the number of charge carriers that could ideally be harvested from a single photon

absorption event is two [7–10]. Moreover, thermalization effects would be decreased and thus the conversion efficiency could be further increased [9], explaining the large interest in SF from the solar cell community. In addition, SF has the potential to double the number of excited states which can take part in a chemical reaction and consequently be of interest for multiphoton/multicharge-carrier processes, e.g. multielectron photocatalysis [11].

For a chromophore to undergo SF certain energy criteria must be fulfilled, namely that $2E(T_1) < E(S_1)$ and $E(S_1) < E(T_2)$. This energetic restriction can partially explain why the number of SF chromophores are relatively small, including but not limited to, acenes, terrylenediimides and 1,3-diphenylisobenzofuran [7, 12–15]. A vast number of studies have shown that efficient SF relies on favorable relative chromophore–chromophore orientation [7, 16–21], for example a slip-stack orientation is the most beneficial for SF in chromophore 6,13-Bis(triisopropylsilylethynyl)pentacen [22]. Moreover, the exact mechanism from initial excitation to free triplet states may differ with the choice of chromophore [14]. SF can occur either as an intermolecular (xSF) or intramolecular (iSF) process [23]. xSF has been observed both in ordered crystals and in highly concentrated (mM) solutions [7, 8, 22, 24]. iSF has been reported in chromophore dimers connected with different types of covalent bridges, whose nature and position of attachment dictates the relative orientation of the chromophores. The length, position of attachment, and electronic properties of the bridge have been investigated thoroughly to understand how through-bond and through-space energy transfer between the two chromophores is affected by the bridge [18, 21, 25–30]. Typically, shorter and/or conjugated bridges result in faster iSF rates than longer bridges. However, this design also risks promoting the undesired fast back-transfer process through triplet-triplet annihilation. Campos and coworkers have reported that through clever dimer design, using homoconjugated bridges, the ratio of forward and backward energy transfer can be optimized to yield more efficient SF materials [28]. Despite these efforts, the efficient separation of the correlated triplet pair into two independent and harvestable triplet states remains a challenge and is an obstacle that must be resolved if efficient utilization of SF materials should be realized [31–33].

To address the challenge of achieving efficient triplet separation while maintaining effective formation of the $^1(TT)$, we explore an alternative chromophore-chromophore coupling strategy based on a dynamic dimer concept. Instead of covalently linking the chromophores together by a covalent bridge, this approach relies on weak intermolecular interactions and equilibrium complex dynamics. We hypothesized that within such a dynamic assembly, formation of the $^1(TT)$ state could still be promoted because the chromophores are in proximity, resembling the interactions observed in many covalently bonded iSF-dimers [18, 21, 25–30, 34]. At the same time, the dynamic nature of these weak intermolecular interactions should assist in dissociation or reorientation of the chromophores and thereby expedite formation of independent triplet excited states. Ideally, this design would reduce triplet-triplet annihilation recombination and relaxation from the $^1(TT)$ to the ground state, while increasing the number of triplet excited states available for harvesting. If successful, it should allow xSF at μM chromophore concentrations.

To test our hypothesis, we chose to study derivatives of the widely used chromophore 6,13-Bis(triisopropylsilylethynyl)pentacen, from now on referred to as TIPS-Pc, as SF has been reported for pentacene derivatives in crystals, films, concentrated solutions, and various covalently linked dimers, [18, 21, 22, 25–30, 35–37]. To promote dynamic dimerization, we synthesized a carboxylic acid functionalized pentacene derivative, 5-(6,13-bis((triisopropylsilyl) ethynyl) pentacen-2-yl) thiophene-2-carboxylic acid (PTCA) along with its corresponding aldehyde analogue, 5-(6,13-bis((triisopropylsilyl) ethynyl) pentacen-2-yl) thiophene-2-carbaldehyde (PTA), shown in figure 1. This functionalization enables us to examine how enhanced intermolecular interactions, particularly hydrogen bonding and π-stacking, affect the photophysical properties relative to the parent TIPS-Pc. Furthermore, the carboxylic acid motif was investigated through deprotonation and metal-ion coordination, where the steady-state and ultrafast dynamics are closely monitored. The hypothesized SF mechanism operating in these suggested dynamic dimers is outlined in scheme 1.

Here we report for the first time a comprehensive photophysical study of PTCA and PTA, including steady-state and time-resolved absorption and photoluminescence (PL). The dynamic dimer concept and the roles of hydrogen bonding and π-stacking were investigated for their influence on SF. From this, we conclude that both PTA and PTCA can undergo SF in solution, even at μM concentrations, and that the rates are tunable by altering the concentration, pH, and addition of zinc cations. While the fundamental photophysical properties of PTA and PTCA are very similar to those of TIPS-Pc, their SF reactivity at low concentrations presents new avenues for SF applications.

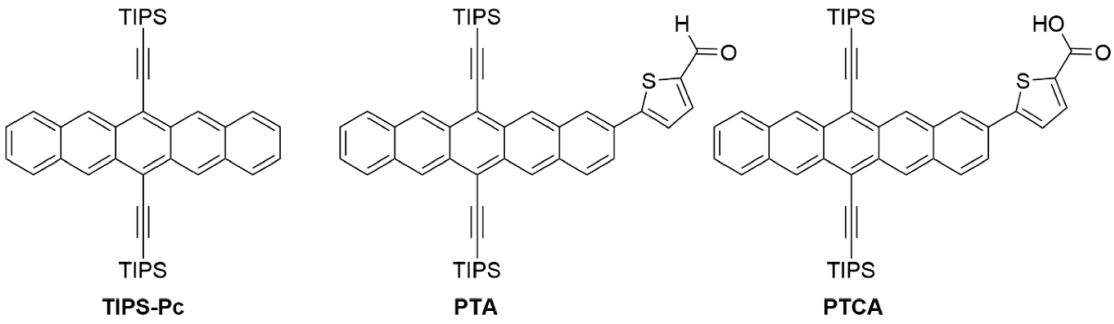

Figure 1. Structures of the reference compound TIPS-Pc and the two chromophores studied in this work, PTA and PTCA.

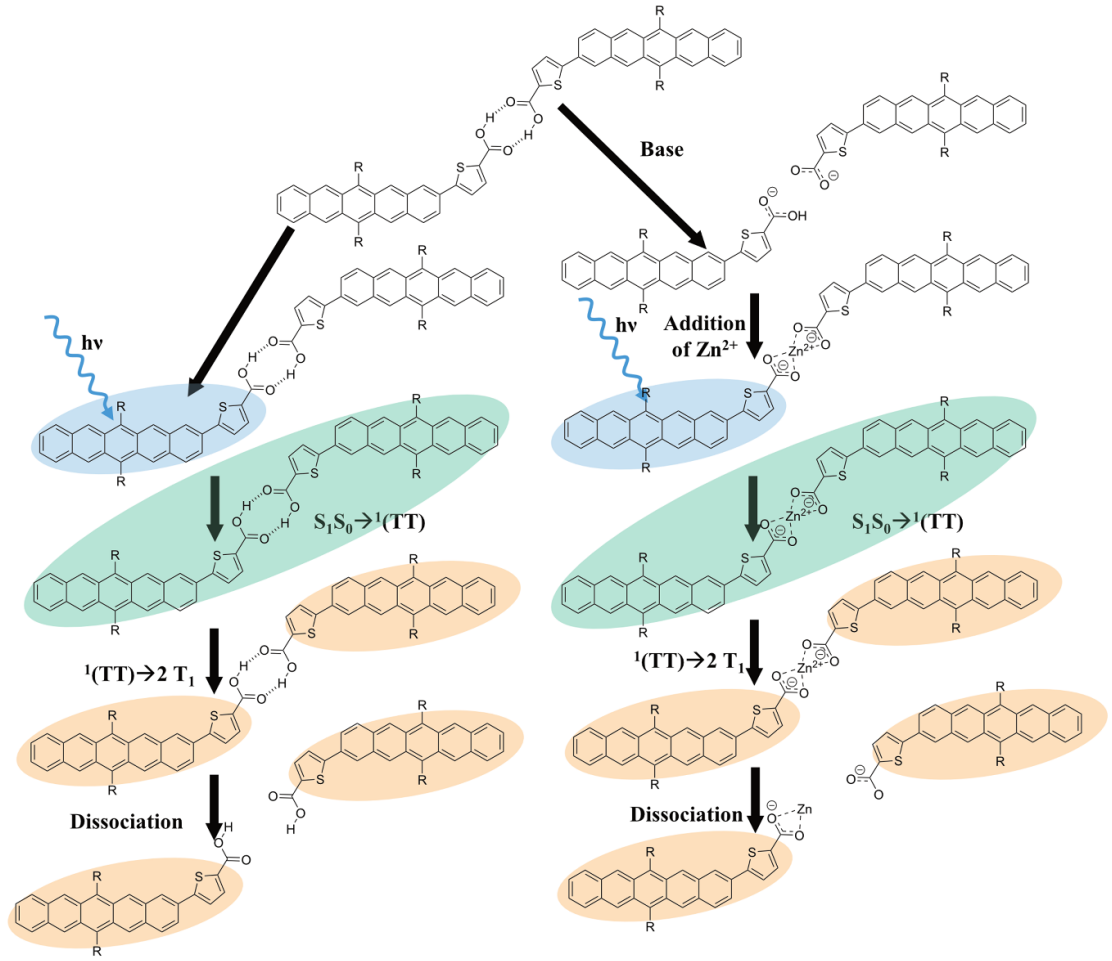

Scheme 1. Schematic illustration of the hypothesis of SF in dynamic dimers. To the left, the dimers are held together through hydrogen bonds or stacking, while to the right, a dynamic ion-bridge by a coordination complex with Zn^{2+} is shown. In the first step, one of the chromophores in the dimer gets excited to its first singlet excited state ($S_0 \rightarrow S_1$). Secondly, a triplet-triplet correlated pair is formed over the dimer ($S_0S_1 \rightarrow {}^1(TT)$). Thirdly, the pair is decorrelated and two triplets, one on each pentacene motif, are formed (${}^1(TT) \rightarrow 2T_1$). Lastly, the two chromophores dissociate and diffuse from each other, facilitating separation of the two triplet excited states. R stand for (triisopropylsilyl) ethynyl.

2. Methods

2.1. Materials

6,13-Bis(triisopropylsilylethynyl)pentacene (TIPS-Pc) and 1,8-diazabicyclo(5.4.0)undec-7-ene (DBU) were purchased from Sigma-Aldrich and used without any purification. Platinum octaethylporphyrin (PtOEP) was purchased from PorphyChem and used as received. $ZnSO_4 \times 7\ H_2O$ was bought from Merck. All reagents used for the synthesis were used without any modifications. Solvents were purchased from Fisher, Fluka and Sigma-Aldrich, and used without further purification.

2.2. Analytical methods

Column chromatography was carried out using Biotage Selekt with Sfär Silica D columns. ^{1}H-NMR spectra were recorded on a Bruker Avance NEO 600 MHz spectrometer. Single-crystal x-ray diffraction (SCXRD) data were collected on a XtaLAB Synergy-R diffractometer equipped with a HyPix detector.

2.3. Photophysical characterization

UV–Vis absorption was measured using a Varian-Cary 50 Bio for routine measurements while a Cary 3500 Multicell or Cary 5000 Spectrophotometer was used for temperature dependent measurements. Steady state PL was collected using a SPEX Fluorolog 3 spectrometer from Jobin Yvon Horiba, with a PMT detector (PFR Technologies). Time resolved PL was recorded using a time-correlated single photon counting (TC-SPC) setup (LifeSpecII, Edinburgh photonics) with a picosecond pulsed diode laser (PDL 800-D, PicoQuant) as excitation source (λ_{exc} = 377 nm, fwhm 50 ps) and an MCP-PMT detector. Quantum yields (Φ) were estimated using the relative method [38] (reference Zn phthalocyanine in DMF). A QuantumDesign Oxford OptistatDN cryostat was used with liquid N_2 to obtain absorption and PL measurements down to 90 K.

2.4. Nanosecond transient absorption (nsTA) measurements

A 10 Hz nanosecond Nd:YAG laser (Quanta-Ray, Spectra-Physics) coupled with an OPO (PrimoScan), was used to generate nanosecond laser pulses, (λ_{exc} = 535 nm, 5–10 ns pulse width, ∼0.2 mW at the sample). Probe light was provided by a halogen lamp (ca 100 mW). Spectra were collected using a CCD camera (iStar, Andor), and single wavelength decays recorded with a fast PMT detector coupled with an oscilloscope (Tektronix TDS2022). Triplet sensitization measurements were carried out using argon-purged samples of platinum octaethylporphyrin (PtOEP) (20 μM) and PTCA or PTA (both 80 μM) in THF and the transient absorption signal were compared to each other.

2.5. Femtosecond transient absorption (fsTA) measurements

A Ti:Sapphire oscillator (Mai-Tai, Spectra-Physics) served as the seeding laser for a regenerative amplifier (Solstice Ace, Spectra-Physics), pumped by an Nd:YLF laser, producing 800 nm laser pulses (ca 60 fs) at a repetition rate of 1 kHz.

An optical parametric amplifier (TOPAS Prime, Light conversion) was used to generate the pump wavelength of 600 nm. Probe light was generated in a CaF_2 crystal and subsequently split into two beams: a reference and a probe, detected via optical fibers connected to a CCD camera (iXon, Andor).

The data was chirp-corrected and analyzed using the open-source python package KimoPack [39]. Prior to the KimoPack processing, outliers, inverted scans and NaN values were corrected or removed.

Low concentration (∼60 μM) samples were measured in a 1 mm quartz cuvette, and high concentration samples (∼10 mM) were measured in custom-made cuvettes described in detail in Supporting information section S2.

2.6. DFT and TD-DFT

DFT gas phase calculations were performed using Gaussian 16 [40], with B3LYP-6-31G** for geometry optimization and CAM-B3LYP-6-31G** for TD-DFT to allow estimation of excitation energies. The Tamm–Dancoff-approximation was employed to obtain better stability of the low-lying triplet excited states [41].

3. Results and discussion

The molecular structure of two molecules studied in this work, PTA and PTCA, alongside the reference compound TIPS-Pc, are shown in figure 1. To evaluate their potential as SF materials, we performed thorough photophysical characterization in a variety of conditions to aid in understanding the fate of the molecules following excitation.

3.1. Synthesis and characterization

Detailed information about the PTA and PTCA synthesis is available in the SI, section S1. Briefly, PTA and PTCA were prepared from a brominated TIPS-pentacene intermediate, according to literature procedures [25, 42], and functionalized to introduce the thiophene-2-carbaldehyde and thiophene-2-carboxylic acid motifs respectively [43]. ^{1}H-NMR confirmed successful synthesis. SCXRD analysis of PTA crystals grown from acetone (CCDC 2499123) revealed a characteristic 1D slip-stacked packing arrangement. The interchromophore geometry is characterized by an interplanar distance (d) of 3.33 Å and

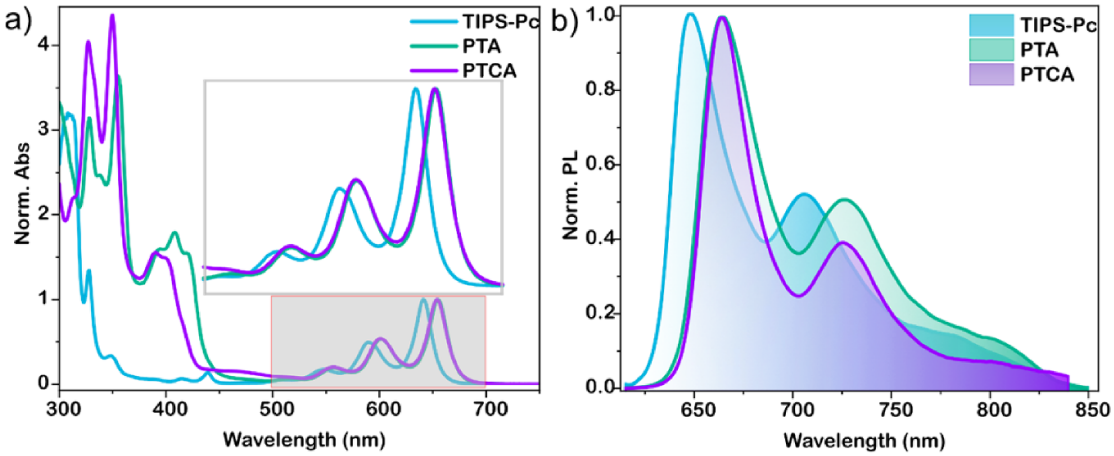

Figure 2. Normalized steady state (a) absorption and (b) photoluminescence of micromolar concentrations of TIPS-Pc, PTCA, and PTA in THF. The inset in (a) shows a magnification of the region 500–700 nm.

a slip angle (θ) of 67.6° (table S1). This is similar to what has been previously observed for TIPS-Pc (3.47 Å) both in packing pattern and interchromophore orientation [44], where strong intermolecular electronic coupling enables efficient SF [45]. While solution-state dynamics introduce substantial rotational freedom, this solid-state packing architecture still indicates a strong thermodynamic preference for a slip-stacked orientation. Consequently, we hypothesize that this geometry serves as a structural model for the transient encounter complexes formed in solution, effectively pre-organizing the chromophores to facilitate the $S_1S_0 \rightarrow {}^1(TT)$ transition.

3.2. Basic photophysical characterization

UV–Vis absorption spectroscopy. Steady-state absorption spectra of PTCA and PTA, figure 2(a) and table 1, were recorded in toluene and THF and compared to TIPS-Pc. Qualitatively, the absorption spectra resemble that of TIPS-Pc albeit with a redshift for the S_0–S_1 transition envelope in the 500–750 nm region. The absorption maximum for the S_0–S_1 transition for PTCA in THF is at 654 nm (656 nm in toluene) and 655 nm for PTA. The maximum for TIPS-Pc is observed at 641 nm, in good agreement with literature values [43]. Moreover, the extinction coefficients are similar to TIPS-Pc, but slightly lower for both functionalized derivatives. Between 450 and 500 nm PTCA exhibits a broad feature, which is not present in the other two compounds, and therefore attributed to the carboxylic acid. Similar features have been observed by Zhang *et al* for carboxylic acid functionalized TIPS-Pentacene [46].

The transition dipole moment of the S_1 transition is oriented along the short axis of the pentacene moiety [49, 50] and functionalization at position 2 is therefore expected to only have minor impact on this absorption band. This is in good agreement with our observations and also DFT calculations where a slight redshift for S_1 is estimated by TD-DFT of 2.24 (554 nm) eV for PTA and PTCA relative to 2.28 eV (544 nm) for TIPS-Pc. Moreover, the T_1 energies were approximated to 0.798, 0.799, and 0.801 eV (1554, 1552, 1548 nm) for PTA, PTCA, and TIPS-Pc, respectively. Thus, SF would remain exothermic for these functionalized chromophores, however with a slightly lower T_1 energy, see SI.

Notable spectral changes in absorption occur below 450 nm, where the weakly allowed S_0–S_2 transition along the long axis of the pentacene unit appears [51]. Upon functionalization, absorption in this region is increased for both PTCA and PTA. As the symmetry is broken, it is expected that this transition can become less forbidden, which has also been reported for other pentacene derivatives functionalized on the same position [27, 46, 52]. Concentration dependent measurements showed no changes in absorption for the two functionalized derivatives when the concentration was varied between 1–100 μM, figure S.14. Furthermore, the temperature dependence of the absorption was investigated, and like for TIPS-Pc, the absorption bands were redshifted at lower temperatures. Additionally, the number of detected vibrational peaks increased and the bandwidths narrowed as the electron–vibron coupling reduced at lower temperatures [53], figure S.20. Based on the steady-state measurements, no large aggregations with significant electronic coupling are believed to be formed as a larger redshift and additional peaks would be expected for close a packed system [54].

Steady state PL. As expected from the UV–Vis results, the PL of PTCA and PTA are also redshifted compared to TIPS-Pc, with vibronic peaks observed at 664 and 727 nm for the thiophene compounds and

Table 1. Photophysical properties of PTCA, PTA and TIPS-Pc in THF and toluene, and PTCA in presence of base.

Sample	λ max absorption (nm) (molar absorptivity ($M^{-1}cm^{-1}$))	λ max PL (nm)	τ Ar (air) (ns)	Φ_{air}
TIPS-Pc (Toluene)	643 (23250)[a], 592, 546, 509, 440, 416, 390, 352, 329, 309	650, 706	—	0.43[b]
PTCA (Toluene)	656, 602, 557, 421, 406, 393, 354, 330	664, 727	—	—
PTCA+ DBU (Toluene)	658, 604, 558, 471 396, 356, 330	671, 730	—	—
TIPS-Pc (THF)	641, 590, 546, 504, 440, 404, 381, 352, 328, 310	648, 707	12.2[c] (7.5)[d]	0.41
PTA (THF)	655 (19100), 602, 557, 515, 423, 408, 396, 355, 328	664, 727	11.2 ± 0.3 (9.4 ± 0.02)	0.30
PTCA (THF)	654 (21000), 601, 555, 469, 400, 391, 350, 326, 311, 294	664, 727	12.7 ± 0.3 (9.9 ± 0.2)	0.34
PTCA+ DBU (THF)	657, 603, 660, 474, 399, 390, 349, 327, 314, 294	674, 731	10.3 (9.2)[e]	0.23

[a]In toluene in μM concentrations, Schaberle FA *et al Chemistry*. 2020; 2(2):545–564 [47].
[b]Compared to 0.75 in air-equilibrated toluene presented by Schaberle *et al Chemistry* 2020, *2*, 545–564 [47].
[c]Choromphore measured with an integrated sphere Dvořák *et al J. Am. Chem. Soc.* 2021, 143, 34, 13 749–13 758 [24].
[d]In THF Alagna *et al J. Phys. Chem. B* 2019, 123(50):10 780–10 793 [48].
[e]No confidence interval was determined.

at 648 and 707 nm for TIPS-Pc respectively, figure 2(b) and table 1. Interestingly, the relative intensity of the vibronic peaks is very similar for TIPS-Pc and PTA, while PTCA appears to have less distortion between the emissive excited state and the ground state. The resemblance between the chromophores confirms the similarities suggested by the PTA crystal structure and TD-DFT. Moreover, the only concentration dependent change in the PL spectra was a relative intensity increase of the second vibrational band at higher concentrations, which is attributed to increased inner filter effects, figure S.14.

PL quantum yields (Φ) of air-equilibrated samples of TIPS-Pc, PTA, and PTCA in THF were estimated using the relative method. PTCA and PTA both exhibit substantially reduced emission quantum yields, around 75% of that of TIPS-Pc, while $\Phi_{TIPS\text{-}Pc}$ is somewhat lower than reported previously by other groups [47]. However, there is variation in the reported literature values and the relative results between the three compounds herein are more important for further discussion than the specific values.

Time-resolved PL. Time-correlated single photon counting of dilute PTA and PTCA samples revealed decays that were satisfactorily modeled with a single exponential decay function. Lifetimes, of 12.7 ± 0.3 and 11.2 ± 0.3 ns (for argon-purged samples) were extracted, respectively, see table 1 and figure S.13, well in agreement with the 12.2 ns reported for TIPS-Pc. Concentration dependent measurements revealed no significant differences in the range 1 μM–100 μM (figure S.18). This result suggests negligible excimer formation at the concentration ranges used as excimer formation would be expected to produce noticeable lifetime changes [24].

Effects of deprotonation of PTCA. To further investigate the role of the carboxylic acid motif for the intermolecular interactions, the photophysics of PTCA was explored in the presence of the organic base,1,8-diazabicyclo 5.4.0 undec-7-ene (DBU). Upon addition of DBU to PTCA, both the absorption and PL display further redshifts, figures 3 and S.15, and the emission bands become broader compared to PTCA in neat solvent. A new spectral feature around 470 nm appears in the absorption spectrum upon addition of base. This is attributed to deprotonated carboxylic acid moieties as suggested by the reduced species spectra extracted from spectroelectrochemical experiments, figures S.10 and S.11, and further supports the assignment of this band to the carboxylic acid.

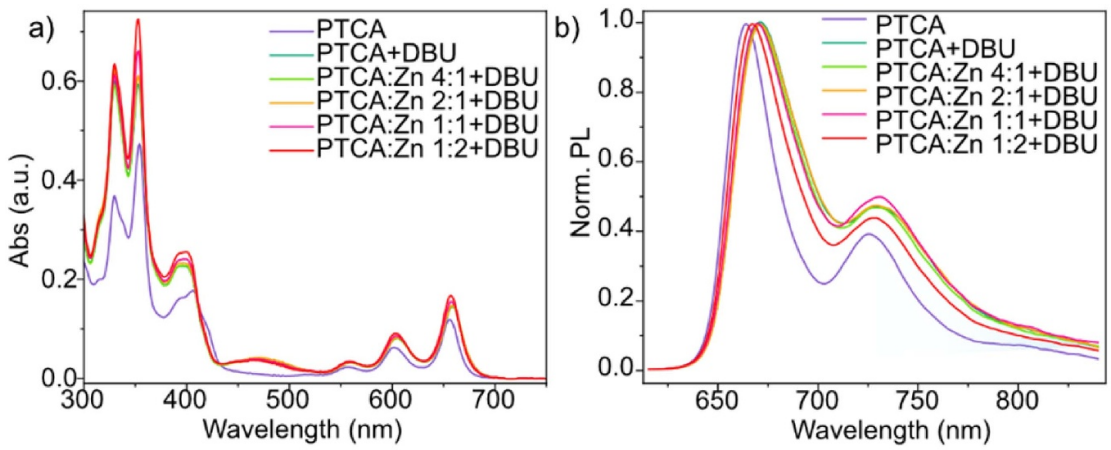

Figure 3. (a) UV–Vis absorption spectra and (b) normalized PL spectra of PTCA in toluene upon addition of DBU and $ZnSO_4$ (in methanol) to PTCA.

In addition, the absorptivity increases across the entire measured region and the second vibronic peak in the emission becomes more pronounced relative to the first peak upon addition of base. This enhancement is attributed to disruption of hydrogen bonds and/or stacking interactions. Moreover, the PTCA emission lifetime decreases in presence of base to 10.3 ns, and the PL quantum yield is reduced to about half of the neutral PTCA, table 1.

Effects of addition of Zn^{2+} to deprotonated PTCA. To evaluate the ability to form dynamic ion-bridges through coordinating two deprotonated PTCAs, Zn^{2+} ions were employed. A Job plot constructed from the UV–Vis titration indicates a 1:2 Zn:PTCA complex in THF, see figure S.15. Only minor changes in the absorption and PL spectra are observed upon zinc addition in figure 3, attributed to substitution at the C-2 position of the pentacene chromophore. As noted, the $S_0 \rightarrow S_1$ transition occurs along the short axis of the pentacene, and coordination is therefore expected to have only a minor impact. PL spectra reveal a slight blueshift relative to the deprotonated species, although still hypsochromic compared to the neutral PTCA. While this shift resembles that of the protonated PTCA, reprotonation is unlikely and is instead credited to Zn^{2+} coordination, decreasing the overall charge. Comparison with anthracene-9-carboxylic acid and the effect of Zn^{2+} addition on its absorption (figure S.16) highlights the impact of the substitution and allows direct evidence of the binding of the Zn^{2+} to the deprotonated carboxylic acid moiety. Furthermore, placement of the carboxylic acid directly on the acene core, along the short axis, leads to significant shifts of the S_1 state.

3.3. Evaluation of PTA and PTCA as SF chromophores

The excited state dynamics of PTCA and PTA were investigated on both long and short timescales and compared to TIPS-Pc to aid spectral assignments. Triplet sensitizing experiments enabled monitoring of the triplet state absorption, allowing direct comparison among the three pentacene derivatives. The long-lived species of PTA and PTCA exhibit broader excited state absorption (ESA) bands than TIPS-Pc, spanning between 400–600 nm (figures S.17 and S.18), suggesting a distribution within the excited-state population with multiple rotamers and molecular arrangements. The characteristic triplet spectral marker for TIPS-Pc appears at 500 nm, whereas for PTA and PTCA it is redshifted to around 520 nm akin to the redshifts observed in the $S_0 \rightarrow S_1$ transition in absorption and emission. The sensitized triplets produced via PtOEP demonstrate triplet lifetimes exceeding 20 μs, figure S.16.

Femtosecond transient absorption of PTA and PTCA. The ultrafast dynamics of the three compounds at relatively low (60 μM) and high concentrations (10 mM) were measured using femtosecond transient absorption following excitation at 600 nm. The transient absorption spectra of PTA and PTCA are presented in figures 4 and 5, respectively. Again, broad ESA bands (400–600 nm) can be observed for all four samples together with the stimulated emission around 660 nm. From TIPS-Pc we know that the $S_1 \rightarrow S_n$ transition is at 450 nm, and triplet formation can be monitored as a shift from the positive

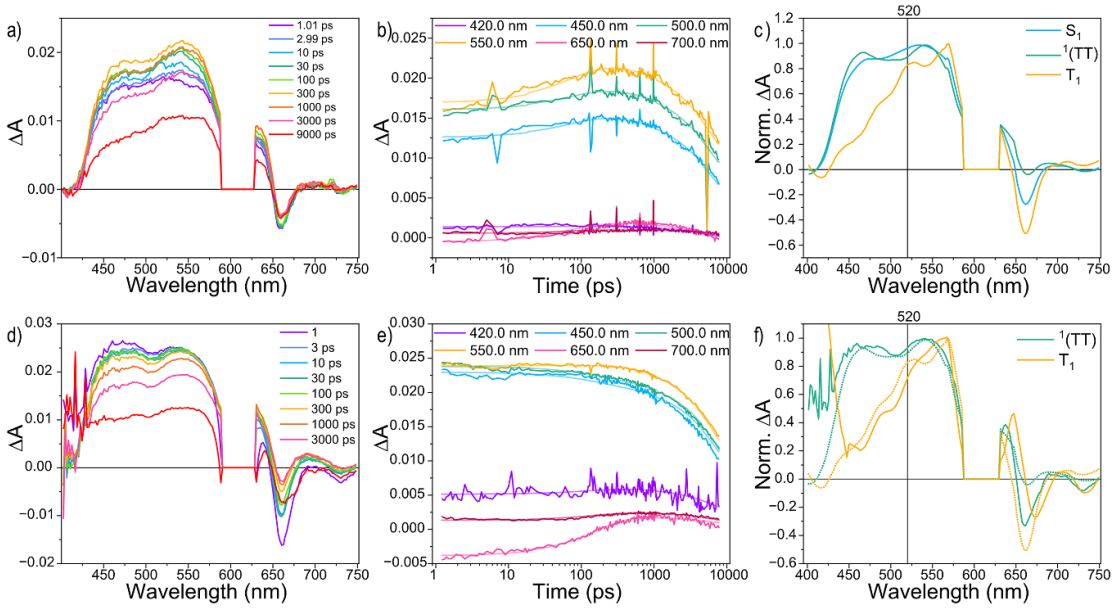

Figure 4. fsTA spectra (a), (c), single wavelength kinetics (b), (d) and species associated spectra (c), (f) of PTA at 60 μM (top) and 10 mM (bottom) in THF. $\lambda_{exc} = 600$ nm. Dashed lines in panel f corresponds to low concentration data.

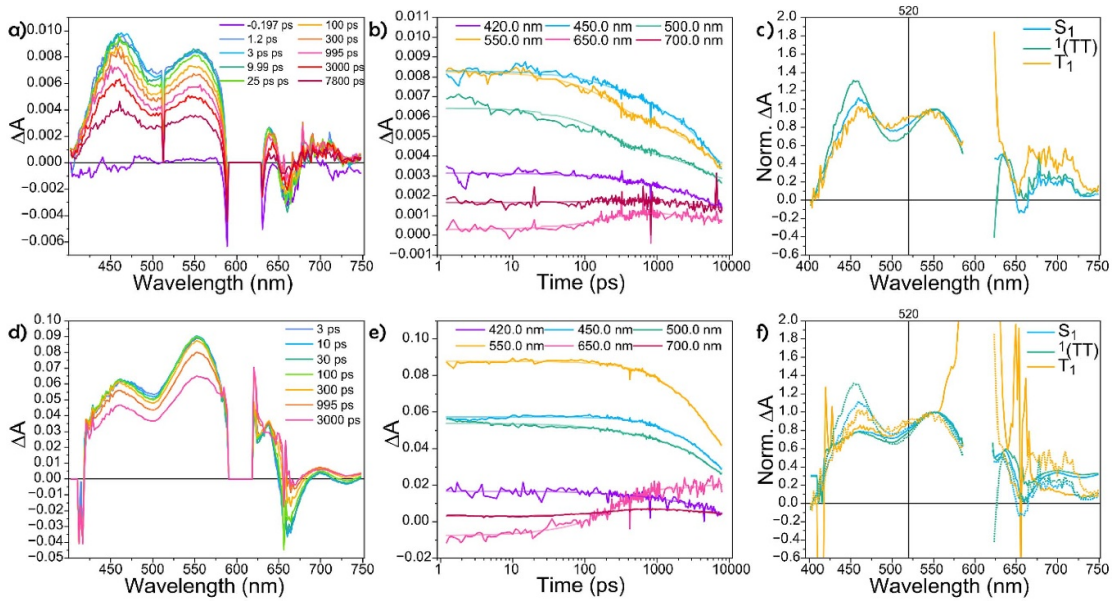

Figure 5. fsTA spectra (a), (c), single wavelength kinetics (b), (d) and species associated spectra (c), (f) of PTCA at 60 μM (top) and 10 mM (bottom) in THF. $\lambda_{exc} = 600$ nm. Dashed lines in panel f corresponds to low concentration data.

peaks at 510 $\rightarrow$ 500 nm. Since the features are wider in the functionalized derivatives, it is more challenging to distinguish specific peaks. However, we can observe fast transitions within the first 100 ps, and a relative increase around 500–550 nm in all cases, indicating triplet formation.

Since no substantial alterations following functionalization were detected in the steady-state measurements, nor in the TDDFT -derived energies, the ultrafast kinetics for the neutral species of PTA and PTCA were initially predicted to follow the same trend as TIPS-Pc. In other words, triplet formation is anticipated to occur only through intersystem crossing (ISC) at low concentrations and at ns time scales, while xSF is expected at mM concentration seen as a rapid formation of a positive signal blue shifted of the initially formed lower energy ESA peak in the fsTA data.

However, the kinetics from the functionalized derivatives deviate from this expectation. At high concentrations, the kinetic behavior is similar across all derivatives, consistent with SF as observed for TIPS-Pc. This supports the conclusion that SF also occurs in the functionalized pentacene derivatives at high

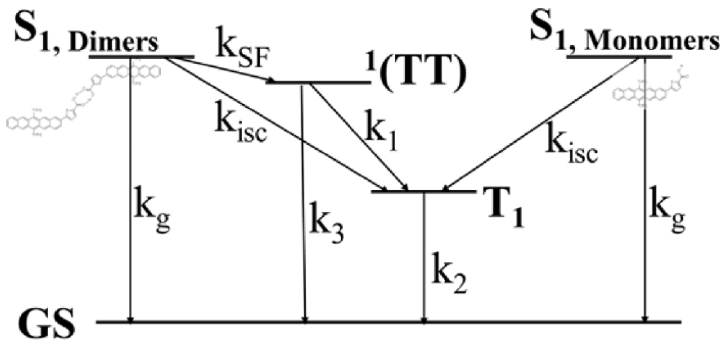

Scheme 2. The kinetic model developed and applied in global fitting of fs-TA data. Excitation of monomeric species is separated by an additional constant representative of the fraction of dimers formed *in situ*.

Table 2. Rates deconvoluted from the fsTA measurements with comparison to literature values of TIPS-Pc[a].

Sample		k_g ($\tau_g = 1/k_g$)[b]	k_{SF} ($\tau_{SF} = 1/k_{SF}$)	k_1 ($\tau_1 = 1/k_1$)	k_3 ($\tau_3 = 1/k_3$)
PTA	High conc	1.1×10^8 (9.4 ns)	4.5×10^{10} (22 ps)	1.3×10^8 (7.6 ns)	5.8×10^7 (17 ns)
	Low conc	1.1×10^8 (9.4 ns)	1.3×10^{11} (8 ps)	1.2×10^8 (8.2 ns)	6.9×10^7 (14 ns)
PTCA	High conc	1.0×10^8 (9.9 ns)	1.0×10^{10} (100 ps)	2.0×10^8 (5.1 ns)	5.7×10^7 (18 ns)
	Low conc	1.0×10^8 (9.9 ns)	5.6×10^{10} (18 ps)	1.7×10^8 (5.9 ns)	5.1×10^7 (20 ns)
PTCA + DBU		1.1×10^8 (9.2 ns)	1.9×10^{11} (5.4 ps)	1.6×10^8 (6.1 ns)	5.3×10^7 (19 ns)
PTCA + DBU+ $ZnSO_4$		1.1×10^8 (9.2 ns)	7.1×10^{10} (14 ps)	9.3×10^7 (101 ns)	1.3×10^8 (18 ns)
TIPS-Pc[c]	High conc	7.7×10^7 (12–13 ns)	$3.8–4.0 \times 10^9$[d]	3.0×10^{11} (3.3 ps)	—
	Dimer	—	$4.2–77 \times 10^{10}$ (1.3–24 ps)	—	$5.0–77 \times 10^9$ (13–200 ps)

[a]All values reported have s^{-1} units unless otherwise noted, in parentheses the lifetimes are presented with the unit s.
[b]Rates estimated based on expected slow k_{isc} in conjunction with measured lifetimes.
[c]High concentration values for TIPS-Pc were taken from [22], with diffusion limited interactivity [24], suggests this estimated rate is of self-quenching not SF. The referenced dimer values were taken from [21] which utilizes covalently bound pentacenes as the dimer for iSF.
[d]Units of M^{-1} s^{-1}.

concentrations. In contrast, when examining the kinetic traces at low concentrations, PTA and PTCA exhibit spectral and temporal features comparable to those observed at mM concentrations. This differs from TIPS-Pc, where SF is diminished at low concentrations due to the low probability of beneficial chromophore–chromophore interactions. We interpret these observations as originating from enhanced intermolecular interactions based on the functionalization, allowing pre-association of the chromophores at low concentrations. To account for this, we developed a kinetic model, see scheme 2. Further justification for this particular model is discussed and justified below. The rates obtained from model are presented in table 2.

At low concentration, the transformation with a <100 ps lifetime was interpreted as SF (k_{SF}) of pre-assembled dimers through intermolecular interactions, presumably hydrogen bonding or stacking resulting in a beneficial orientation and electronic coupling. This assignment relies on the premise that no other transitions from the S_1 proceed at comparable rates (1.3×10^{11} s^{-1} for PTA, and 5.6×10^{10} s^{-1} for PTCA), supported by the spectral shifts discussed further below, and by comparisons across the different samples. Moreover, similar rates for iSF in pentacene dimers have been reported previously

[25, 27–30]. The initial formation of the $^1(TT)$ state is faster in PTA than in PTCA, the relative efficiency is supported by the Φ_{PL} where PTA showed a lower yield compared to PTCA, table 1. This indicates more prominent intermolecular interactions or beneficial chromophore-chromophore alignment and alternative decay pathways of the singlet state in PTA.

At higher concentrations, however, contrary to expectations, the iSF rate decreased for both PTA and PTCA. In PTA k_{SF} was slowed to a rate with a corresponding lifetime of 22 ps, compared to 8 ps at low concentrations, table 2. PTCA formation was drastically reduced with a new lifetime of 100 ps, from 18 ps at low concentrations. Subsequent to the SF process, in both high and low concentration, relaxation/separation to free triplet states from the correlated triplet pair occurred on a 5–9 ns timescale (k_1), slightly faster than the above reported singlet relaxation to the ground state.

The species associated spectra (SAS) procured through global analysis corresponding to these excited states are depicted in figures 4(c) and (f) for PTA and figures 5(c) and (f) for PTCA, respectively. The SAS extracted from both high and low concentration of PTA are in reasonable agreement with the sensitized spectra displayed in figure S.12, supporting the assigned rate and species within the model. Moreover, the spectral shifts are closely consistent with previous experimental measurements of pentacene systems, including dimeric structures [18, 21]. The spectral change from the S_1S_0 to $^1(TT)$ involves a blue shift and growth of the higher energy transition around 450 nm relative to the counterpart at 550 nm, which can be observed in the SAS. The exception to this is for high concentration PTCA, figure 5(f), where little change other than loss of signal between peaks is observed at early times, figure 5(e). The spectra associated with the residual signal interpreted here as a free triplet in all cases resulted in the growth of a new peak around 515–525 nm, the characteristic band of the free triplet. The remaining triplet state did not decay to any substantial degree within the measured time range, supported by the sensitized triplet measurements. For applications in which triplet harvesting is the main primary goal, the longevity of the triplets is crucial. Although a detailed study of triplet extraction or harvesting is beyond the scope of this work, it is, as noted earlier, a key motivation to improve the triplet separation.

It should be pointed out that 'dimer' in the kinetic model is a way to estimate how much of the population that undergoes SF and should not be interpreted as a true measure of the amount of dimers. In practice the dimer fraction is projected by iterative fitting of a locked fraction to reduce the risk of overparameterization (see details in section S5.3). Thus, a measure of how much of the total chromophore concentration is estimated to undergo SF can be obtained. For PTA at low concentrations, at least 15% is in assemblies in a beneficial orientation and electronic coupling to result in SF. This ratio is only 10% for PTCA suggesting a less advantageous orientation, rather than a lower dimerization constant.

From this, an approximate overall triplet yield was generated to ∼25% for the low concentrations, and 110%–130% at high concentrations (S5.5). This is substantially lower than values previously reported of covalently bound dimers [27, 28], but this inherently from the dynamic equilibriums where not all chromophores are in dimers. SF yields up to 200% at low concentrations is therefore unrealistic. Calibrated triplet yield measurements would provide an important basis for assessing the validity of our estimates but are left for future investigations.

Effects of deprotonation of PTCA. Through addition of base to a low concentration sample of PTCA, changes in the excited-state absorption can be seen immediately after excitation. The transition centered around 550 nm is further broadened, figures 6(a)–(c). A transformation on the order of 1.9×10^{11} can be observed, resulting in a relative increase in intensity and blue-shifting of the 450 nm band. The same changes are observed in the formation of the $^1(TT)$ in the absence of base, figures 5(a)–(c), which in conjunction with the 5 ps transformation assists in the assignment of this intermediate $^1(TT)$ species.

As hydrogen bonding dimerization is expected to be limited following the addition of the base, an increase in monomer concentration is predicted with a reduced degree of SF. The overall spectral characteristics and the kinetics do indeed more closely resemble those of low concentration TIPS-Pc control samples. Still, through iterative fittings with varying 'dimer fraction', the best fit was obtained when 65% of the total chromophore concentration was assigned to undergo SF, substantially higher than for the neutral PTCA of 10% (S5.3). In particular, this assignment was supported by the observation of the formed triplet species with the predicted 520 nm band. Moreover, the k_{SF} is increased compared to before deprotonation. We postulate the possibility of increased favorable intermolecular orientation via the newly generated dipole in a relative non-polar solvent as the origin of the increased k_{SF}, and a higher dimer fraction. Potentially resulting from increased stacking of the monomers conducive to rapid formation of the correlated triplet pair or an excimer state.

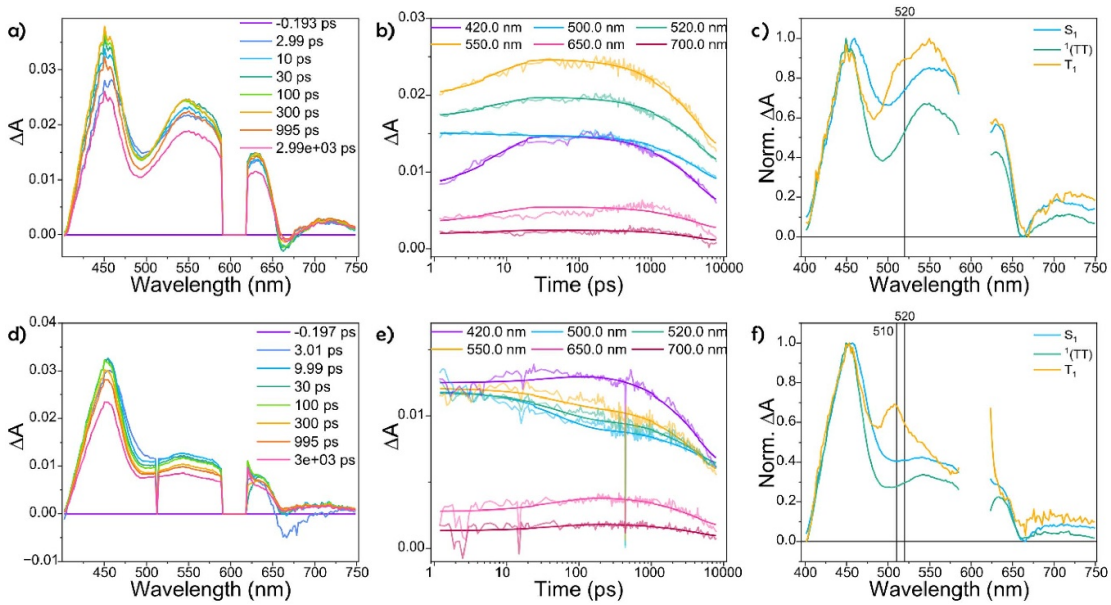

Figure 6. fsTA spectra (a), (c), single wavelength kinetics (b), (d) and species associated spectra (c), (f) of PTCA at 60 μM with base (top) and with base and Zn^{2+} (bottom) in THF. $\lambda_{exc} = 600$ nm.

Effects of addition of Zn^{2+} to deprotonated PTCA. As hypothesized at the outset, the inclusion of a coordinating metal could promote dynamic binding/encounter complexes prior to excitation to improve the chances of SF at low concentrations. However, similar to when base is added, we see one rapid exchange displayed as a blueshift and growth at 450 nm, figures 6(d)–(f), with a lifetime of 14 ps, with a similar to the SF lifetime of neutral PTCA. This observation supports a hypothesis in which the Zn^{2+} ions are able to orient the molecules in a particular way in which SF is possible. Unfortunately, the decorrelation of $^1(TT)$ is noticeably slower, and in turn the direct transition to the ground state, k_3, becomes more influential. Thus, SF is actually less promoted than when the chromophores are free to align as they choose. Indeed, as depicted, the use of the Zn^{2+} ion could result in substantial electronic decoupling between two chromophores, while simultaneously extending the bridge. Expanding the bridge within dimeric systems has previously been shown to reduce the iSF rates [25]. From the SAS in figures 6(f) and (a) more pronounced peak at 510 nm for the triplet is observed, indicating there is a more homogenous configuration of the dimers compared to the freely associated PTCA (figure 5). Structural or computational studies would be needed for confirming the chromophore orientation and electronic coupling.

Equilibrium constants for the two associations in the formation of a $Zn^{2+}[PTCA^-]_2$ complex has not been established since only small spectral shifts in the steady-state could be detected (figure 3). However, from the 0.6 fraction of dimers obtained by the kinetic model, a dimerization constant of 1.5×10^3 can be used as a ballpark value. The ultrafast dynamics were measured for different zinc to PTCA ratios, but no substantial effect of concentration could be identified in the kinetics. Solubility and the choice of solvent is an important concern as it can greatly affect the intermolecular interactions, deprotonation, ion interactions, and equilibrium constants. THF was selected to have a solvent with both polar and non-polar abilities, still $ZnSO_4$ had to be pre-dissolved in methanol before further dilution in THF. Thus, extending the study to other ions with stronger or other coordination orientations can be challenging, yet intriguing as it can affect the chromophore-chromophore interaction and thereby alter the SF rates and possibilities.

Kinetic model justification. In the following section, a justification and more substantial background to the kinetic model is given. As previously mentioned, based on spectral and temporal comparison the kinetic model was developed to simulate the ultrafast transient absorption data collected and is outlined in scheme 2. In figure 7 the kinetic traces at the wavelengths where triplet formation is expected can be compared for all the eight samples discussed previously.

Herein, a partial dimer formation of the chromophores is included in the model, where SF is assumed to only occur in these configurations where dimerization or proximity via encounter complexes is established prior to excitation, and their resulting orientation is beneficial. Orbital overlap and

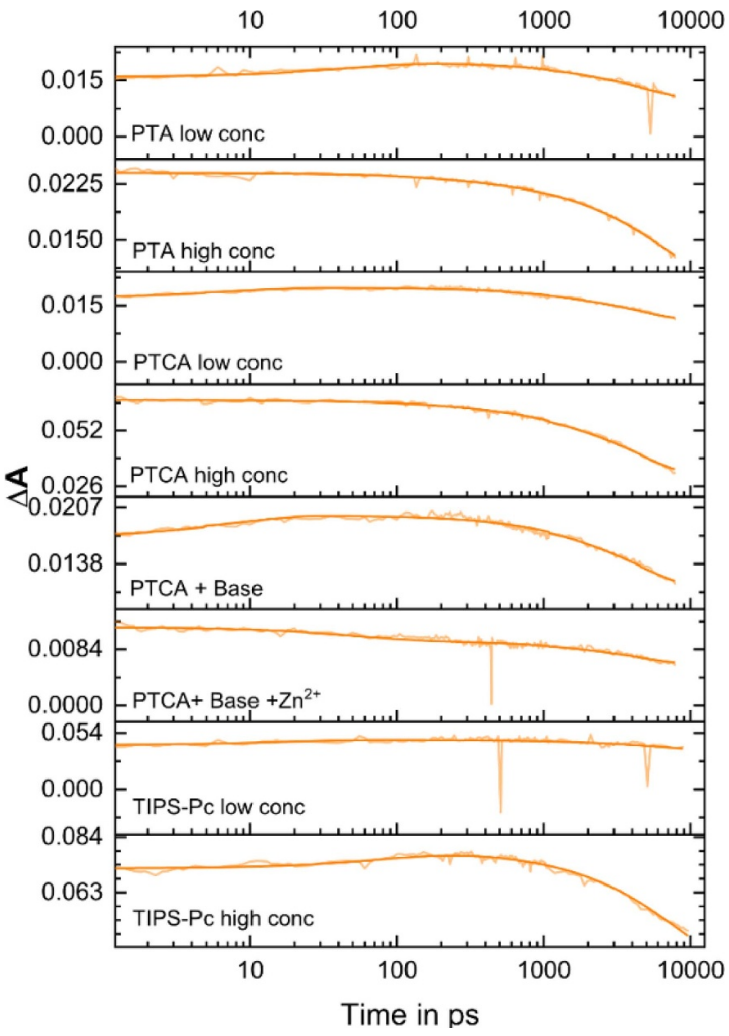

Figure 7. Kinetic traces from top to bottom panels: PTA, and PTCA (at 520 nm) in THF at 60 μM ('Low Conc') in a 2 mm cuvette, and 10 mM concentrations ('High Conc') in a ∼100 μm thin homemade cuvette, respectively, followed by PTCA + DBU, and PTCA + DBU + Zn (at 520 nm), and lastly in the two lower panels TIPS-Pc (at 510 nm) at 60 μM and 10 mM. The raw data is shown in the lighter color and the resulted model in the darker shade. For the TIPS-Pc samples a sequential model with two rate constants is used while for the others the model outlined in scheme 2 is operated.

chromophore–chromophore coupling are necessary for SF to be achieved, and no other explanation is found that satisfies the notion except formation of assemblies. Moreover, the rates are similar to those of iSF observed in covalently linked dimers [18, 21, 27, 28, 30]. Through iteration of a dimer fraction or concentration of species with access to SF a predicted level of dimerization could be estimated. The degree of preassembled aggregates and encounter complexes are approximated to be below 25% for the 60 μM, with the highest degree of fit at ∼10% for PTCA and ∼15% for PTA, and greater than 80% for the high concentration. This indicates a concentration sensitive equilibrium and a dimerization constant of $\sim 1.7 \times 10^4$ to $2.2\ 10^2$ M^{-1}, which can be compared to the equilibrium constant for dimerization of benzoic acid in n-heptane (1.59×10^4 M^{-1}) [55].

Consequently, a fraction of the total population cannot undergo SF as they are not close enough or are in a non-beneficial conformation, these are described as monomers in scheme 2. Triplet formation can still be possible from these species by direct ISC, outlined as k_{ISC} from the S_1 state of monomers in scheme 2. Moreover, the triplet population can be further populated by ISC from the dimers and through separation of the $^1(TT)$ state succeeding xSF from the non-covalent assemblies. For the high concentrated samples, a simple sequential model can also be applied as for high concentration of TIPS-Pc, see S5.1, as the dimer concentration in the model goes towards unity it is expected SF would happen both in preassembled and freely diffusing systems.

Decay from the triplet state, k_2, and ISC from the native singlet, k_{isc}, are included in the model but cannot be resolved within the fs-TA temporal limits. Decorrelation from $^1(TT)$ state is assumed to be

occurring substantially faster than ISC. This is based on estimations from the emission quantum yields and lifetimes presented in table 1 and previous literature which estimates a k_{isc} of 91 ns [22].

In our analysis, we assume a direct conversion from the S_1S_0 in the dimers to $^1(TT)$ via k_{SF}, without the formation of an intermediate with charge-transfer character (CT). Deprotonation and spectroelectrochemistry measurements indicate that a CT state would manifest as a rise near 450 nm in the fsTA spectra; however, no growth of such signature is detected in the fsTA measurements and consequently, a CT state is not included in the kinetic model. It has however been showcased in other systems that these states can be profoundly prominent for SF processes [15, 26, 56, 57]. In this regard we do recognize the possibility that we have the state we have assigned as S_1S_0 is actually a CT state due to previously reported sub-ps formation, partially supported by the increased relative intensity at roughly 450–460 nm for the higher expected dimer fraction samples, including the difference in signal for high and low concentration. Excimer formation as an intermediate or an alternative decay pathway has been considered but rejected as an influential photophysical process in these systems. A more substantial concentration dependency on rates would be expected than what is observed herein. In the literature, there are vastly different opinions and kinetic models presented regarding this subject for SF materials [12, 22, 24, 58–60].

The addition of a thiophene together with an aldehyde and carboxylic acid, respectively, was selected to improve the interactions by promoting stacking of the thiophene groups and hydrogen bonding, without severely affecting the energy landscape of the pentacene core. The exact intermolecular interactions between the chromophores are not known. Potentially, there might be a combination of several different interactions, resulting in a distribution of conformations, which might be an explanation to the broad spectral features seen in the time-resolved data. Since there are no indications of large aggregations, dimerization is therefore the most probable intermolecular interaction. Where hydrogen bonds between two carboxyl acids are expected to be the strongest interaction, followed by aldehyde-aldehyde, and carboxyl-thiophene interactions [61, 62]. The type, strength and orientation of the intermolecular bonds are critical as it determines the orientation and distance of the pentacene motifs, governing the SF process and triplet separation. Here, more extensive computational modeling might provide useful information about these interactions in the future.

4. Conclusion

Two functionalized pentacene chromophores were successfully synthesized, and a thorough photophysical investigation has been accomplished. The introduction of a thiophene unit results in a redshift in absorption and emission, decreased quantum yields and emission lifetimes. Furthermore, intermolecular interactions are enhanced as evident in both the steady-state and transient absorption and emission. These multimers enable new excited-state decay pathways, ascribed to SF facilitated by the close proximity of the pentacene moieties. Comparing PTCA with PTA, they showcase similar photophysical properties but boosted SF for the PTA, where a lower emission quantum yield also could be observed.

The rates for SF have been modulated and calculated to occur with 10–100 ps lifetimes at high concentrations and on the order of 8–18 ps at micromolar concentrations. Moreover, deprotonation and addition of Zn^{2+} with sequential coordination alters the rates, demonstrating that the photophysics can be substantially altered through simple chemical adjustments such as changing the pH, or addition of cations.

Importantly, the functionalization strategy enables efficient SF in solutions even at low concentrations ($<$100 μM), which is not achievable with unmodified pentacene. Introducing many new opportunities for solution-phase-applications and provides a versatile platform for further molecular design with many interesting avenues.

Acknowledgments

This work was partially supported by the Wallenberg Initiative Materials Science for Sustainability (WISE) funded by the Knut and Alice Wallenberg Foundation. Chalmers materials analysis lab (CMAL) is acknowledged for SCXRD analysis. Chalmers AoA Nano for funding for MB and ABM. MA thanks the Swedish Research Council Vetenskapsrådet Grant Number 2020-04335 for financial support. We thank Professor Bo Albinsson for help with DFT calculations.

Data availability statement

All data that support the findings of this study are included within the article (and any supplementary files).

Supplementary information available at: https://doi.org/10.1088/2515-7639/ae9191/data1.

Contribution report

H L did all the photochemical experiments and majority of the analysis, and majority of the writing. H M performed synthesis, cyclic voltammetry, and spectroelectrochemical measurements. M G and H M collected the crystal structure data and refined the structure. A B M did initial experiments, fsTA analysis. The project was conceived, designed and supervised by M A and A B M. A B M and M A also contributed to writing the paper.

ORCID iDs

Hanna Larsson 0009-0000-7994-1417
Hassan Mourad 0000-0001-8565-1379
Andrew B Maurer 0000-0002-4147-0290
Maria Abrahamsson 0000-0002-6931-1128

References

[1] IEA 2025 *Renewables 2025* pp 11–17
[2] Haegel N M and Kurtz S R 2021 Global progress toward renewable electricity: tracking the role of solar *IEEE J. Photovolt.* **11** 1335–42
[3] Shockley W and Queisser H J 1961 Detailed balance limit of efficiency of p-n junction solar cells *J. Appl. Phys.* **32** 510–9
[4] Dexter D L 1979 Two ideas on energy transfer phenomena: ion-pair effects involving the OH stretching mode, and sensitization of photovoltaic cells *J. Lumin.* **18-19** 779–84
[5] Baldacchino A J, Collins M I, Nielsen M P, Schmidt T W, McCamey D R and Tayebjee M J Y 2022 Singlet fission photovoltaics: progress and promising pathways *Chem. Phys. Rev.* **3** 021304
[6] Hanna M C and Nozik A J 2006 Solar conversion efficiency of photovoltaic and photoelectrolysis cells with carrier multiplication absorbers *J. Appl. Phys.* **100** 074510
[7] Smith M B and Michl J 2010 *Chem. Rev.* **110** 6891–936
[8] Singh S, Jones W J, Siebrand W, Stoicheff B P and Schneider W G 1965 Laser generation of excitons and fluorescence in anthracene crystals *J. Chem. Phys.* **42** 330–42
[9] Carrod A J, Gray V and Börjesson K 2022 Recent advances in triplet–triplet annihilation upconversion and singlet fission, towards solar energy applications *Energy Environ. Sci.* **15** 4982–5016
[10] Gray V, Weiss L and Rao A 2022 Singlet fission: mechanisms and molecular design *Emerging Strategies to Reduce Transmission and Thermalization Losses in Solar Cells: Redefining the Limits of Solar Power Conversion Efficiency* ed J S Lissau and M Madsen (Springer) pp 291–311
[11] Wang T, Liu H, Wang X, Tang L, Zhou J, Song X, Lv L, Chen W, Chen Y and Li X 2023 Employing singlet fission into boosting the generation of singlet oxygen and superoxide radicals for photooxidation reactions *ACS Catal.* **13** 13902–11
[12] Johnson J C and Michl J 2017 1,3-diphenylisobenzofuran: a model chromophore for singlet fission *Top. Curr. Chem.* **375** 80
[13] Schrauben J N, Ryerson J L, Michl J and Johnson J C 2014 Mechanism of singlet fission in thin films of 1,3-diphenylisobenzofuran *J. Am. Chem. Soc.* **136** 7363–73
[14] Smith M B and Michl J 2013 Recent advances in singlet fission *Annu. Rev. Phys. Chem.* **64** 361–86
[15] Margulies E A, Miller C E, Wu Y, Ma L, Schatz G C, Young R M and Wasielewski M R 2016 Enabling singlet fission by controlling intramolecular charge transfer in π-stacked covalent terrylenediimide dimers *Nat. Chem.* **8** 1120–5
[16] Korovina N V, Pompetti N F and Johnson J C 2020 Lessons from intramolecular singlet fission with covalently bound chromophores *J. Chem. Phys.* **152** 040904
[17] Girija A V, Zeng W, Myers W K, Kilbride R C, Toolan D T W, Zhong C, Plasser F, Rao A and Bronstein H 2024 Singlet fission in Pechmann dyes: planar chromophore design and understanding *J. Am. Chem. Soc.* **146** 18253–61
[18] Zirzlmeier J, Lehnherr D, Coto P B, Chernick E T, Casillas R, Basel B S, Thoss M, Tykwinski R R and Guldi D M 2015 Singlet fission in pentacene dimers *Proc. Natl Acad. Sci. USA* **112** 5325–30
[19] Wang L, Olivier Y, Prezhdo O V and Beljonne D 2014 Maximizing singlet fission by intermolecular packing *J. Phys. Chem. Lett.* **5** 3345–53
[20] Zimmerman P M, Musgrave C B and Head-Gordon M 2013 A correlated electron view of singlet fission *Acc. Chem. Res.* **46** 1339–47
[21] Ringström R, Edhborg F, Schroeder Z W, Chen L, Ferguson M J, Tykwinski R R and Albinsson B 2022 Molecular rotational conformation controls the rate of singlet fission and triplet decay in pentacene dimers *Chem. Sci.* **13** 4944–54
[22] Walker B J, Musser A J, Beljonne D and Friend R H 2013 Singlet exciton fission in solution *Nat. Chem.* **5** 1019–24

[23] Sanders S N, Kumarasamy E, Pun A B, Steigerwald M L, Sfeir M Y and Campos L M 2016 Intramolecular singlet fission in oligoacene heterodimers *Angew. Chem., Int. Ed.* **55** 3373–7
[24] Dvořák M *et al* 2021 Singlet fission in concentrated TIPS-pentacene solutions: the role of excimers and aggregates *J. Am. Chem. Soc.* **143** 13749–58
[25] Sanders S N *et al* 2015 Quantitative intramolecular singlet fission in bipentacenes *J. Am. Chem. Soc.* **137** 8965–72
[26] Bo Y, Hou Y, Lavergne D A X, Clark T, Ferguson M J, Tykwinski R R and Guldi D M 2025 Reversible gating of singlet fission by tuning the role of a charge-transfer state *Nat. Commun.* **16** 2968
[27] Parenti K R, He G, Sanders S N, Pun A B, Kumarasamy E, Sfeir M Y and Campos L M 2020 Bridge resonance effects in singlet fission *J. Phys. Chem. A* **124** 9392–9
[28] Kumarasamy E *et al* 2017 Tuning singlet fission in π-bridge-π chromophores *J. Am. Chem. Soc.* **139** 12488–94
[29] Fuemmeler E G *et al* 2016 A direct mechanism of ultrafast intramolecular singlet fission in pentacene dimers *ACS Cent. Sci.* **2** 316–24
[30] Sakai H, Inaya R, Nagashima H, Nakamura S, Kobori Y, Tkachenko N V and Hasobe T 2018 Multiexciton dynamics depending on intramolecular orientations in pentacene dimers: recombination and dissociation of correlated triplet Pairs *J. Phys. Chem. Lett.* **9** 3354–60
[31] Pensack R D, Ostroumov E E, Tilley A J, Mazza S, Grieco C, Thorley K J, Asbury J B, Seferos D S, Anthony J E and Scholes G D 2016 Observation of two triplet-pair intermediates in singlet exciton fission *J. Phys. Chem. Lett.* **7** 2370–5
[32] Pun A B, Asadpoordarvish A, Kumarasamy E, Tayebjee M J Y, Niesner D, McCamey D R, Sanders S N, Campos L M and Sfeir M Y 2019 Ultra-fast intramolecular singlet fission to persistent multiexcitons by molecular design *Nat. Chem.* **11** 821–8
[33] Wang Z *et al* 2021 Free-triplet generation with improved efficiency in tetracene oligomers through spatially separated triplet pair states *Nat. Chem.* **13** 559–67
[34] Hayasaka R, Sakai H, Fuki M, Okamoto T, Khan R, Higashi M, Tkachenko N V, Kobori Y and Hasobe T 2024 The effect of torsional motion on multiexciton formation through intramolecular singlet fission in ferrocene-bridged pentacene dimers *Angew. Chem., Int. Ed.* **63** e202315747
[35] Krishnapriya K C, Roy P, Puttaraju B, Salzner U, Musser A J, Jain M, Dasgupta J and Patil S 2019 Spin density encodes intramolecular singlet exciton fission in pentacene dimers *Nat. Commun.* **10** 33
[36] Duan H-G *et al* 2020 Intermolecular vibrations mediate ultrafast singlet fission *Sci. Adv.* **6** eabb0052
[37] Basel B S *et al* 2017 Unified model for singlet fission within a non-conjugated covalent pentacene dimer *Nat. Commun.* **8** 15171
[38] Lakowicz J R 2006 *Principles of Fluorescence Spectroscopy* 3rd edn (Springer)
[39] Müller C, Pascher T, Eriksson A, Chabera P and Uhlig J 2022 KiMoPack: a python package for kinetic modeling of the chemical mechanism *J. Phys. Chem. A* **126** 4087–99
[40] Frisch M J *et al* 2016 *Gaussian 16 Rev. C.01*
[41] Hirata S and Head-Gordon M 1999 Time-dependent density functional theory within the Tamm–Dancoff approximation *Chem. Phys. Lett.* **314** 291–9
[42] Plunkett K N, Godula K, Nuckolls C, Tremblay N, Whalley A C and Xiao S 2009 Expeditious synthesis of contorted hexabenzocoronenes *Org. Lett.* **11** 2225–8
[43] Li Z *et al* 2011 Functionalized pentacenes for dye-sensitized solar cells *J. Photon. Energy* **1** 011106
[44] Anthony J E, Brooks J S, Eaton D L and Parkin S R 2001 Functionalized pentacene: improved electronic properties from control of solid-state order *J. Am. Chem. Soc.* **123** 9482–3
[45] Pensack R D*et al* 2018 Striking the right balance of intermolecular coupling for high-efficiency singlet fission *Chem. Sci.* **9** 6240-59 (available at: https://pubs.rsc.org/sc/article/9/29/6240/621763/Striking-the-right-balance-of-intermolecular)
[46] Zhang J, Sakai H, Suzuki K, Hasobe T, Tkachenko N V, Chang I-Y, Hyeon-deuk K, Kaji H, Teranishi T and Sakamoto M 2021 Near-unity singlet fission on a quantum dot initiated by resonant energy transfer *J. Am. Chem. Soc.* **143** 17388–94
[47] Schaberle F A, Serpa C, Arnaut L G, Ward A D, Karlsson J K G, Atahan A and Harriman A 2020 The photophysical properties of triisopropylsilyl-ethynylpentacene—a molecule with an unusually large singlet-triplet energy gap—in solution and solid phases *Chemistry* **2** 545–64
[48] Alagna N *et al* 2019 Singlet fission in tetraaza-TIPS-pentacene oligomers: from fs excitation to μs triplet decay via the biexcitonic state *J. Phys. Chem. B* **123** 10780–93
[49] Haas S, Matsui H and Hasegawa T 2010 Field-modulation spectroscopy of pentacene thin films using field-effect devices: reconsideration of the excitonic structure *Phys. Rev. B* **82** 161301
[50] Tiago M L, Northrup J E and Louie S G 2003 Ab initio calculation of the electronic and optical properties of solid pentacene *Phys. Rev. B* **67** 115212
[51] Trinh M T, Pinkard A, Pun A B, Sanders S N, Kumarasamy E, Sfeir M Y, Campos L M, Roy X and Zhu X-Y 2017 Distinct properties of the triplet pair state from singlet fission *Sci. Adv.* **3** e1700241
[52] Paul S, Govind C and Karunakaran V 2021 Planarity and length of the bridge control rate and efficiency of intramolecular singlet fission in pentacene dimers *J. Phys. Chem. B* **125** 231–9
[53] Meyenburg I, Breuer T, Karthäuser A, Chatterjee S, Witte G and Heimbrodt W 2016 Temperature-resolved optical spectroscopy of pentacene polymorphs: variation of herringbone angles in single-crystals and interface-controlled thin films *Phys. Chem. Chem. Phys.* **18** 3825–31
[54] Tayebjee M J Y, Schwarz K N, MacQueen R W, Dvořák M, Lam A W C, Ghiggino K P, McCamey D R, Schmidt T W and Conibeer G J 2016 Morphological evolution and singlet fission in aqueous suspensions of TIPS-pentacene nanoparticles *J. Phys. Chem. C* **120** 157–65
[55] Kubista M, Sjoeback R and Albinsson B 1993 Determination of equilibrium constants by chemometric analysis of spectroscopic data *Anal. Chem.* **65** 994–8
[56] Cui B, Jha A and Duan H-G 2024 Interplay of intermolecular and intramolecular vibrations mediates ultrafast singlet fission *J. Phys. B: At. Mol. Opt. Phys.* **57** 105101
[57] Ito S, Nagami T and Nakano M 2015 Density analysis of intra- and intermolecular vibronic couplings toward bath engineering for singlet fission *J. Phys. Chem. Lett.* **6** 4972–7
[58] Basel B S, Hetzer C, Zirzlmeier J, Thiel D, Guldi R, Hampel F, Kahnt A, Clark T, Guldi D M and Tykwinski R R 2019 Davydov splitting and singlet fission in excitonically coupled pentacene dimers *Chem. Sci.* **10** 3854–63

[59] Hausch J, Berges A J, Zeiser C, Rammler T, Morlok A, Bredehöft J, Hammer S, Pflaum J, Bardeen C J and Broch K 2022 Distinguishing between triplet-pair state and excimer emission in singlet fission chromophores using mixed thin films *J. Phys. Chem. C* **126** 6686–93
[60] Buchanan E A *et al* 2021 Competing singlet fission and excimer formation in solid fluorinated 1,3-diphenylisobenzofurans *J. Phys. Chem. C* **125** 27058–71
[61] Atkins P, De paula J and Friedman R 2014 *Physical Chemistry: Quanta, Matter, and Change* 2nd edn (Oxford University Press)
[62] Saragi R T, Juanes M, Pérez C, Pinacho P, Tikhonov D S, Caminati W, Schnell M and Lesarri A 2021 Switching hydrogen bonding to π-stacking: the thiophenol dimer and trimer *J. Phys. Chem. Lett.* **12** 1367–73